Invited Paper

Low-noise high-electron-mobility-transistor terahertz detector integrated with bow-tie antenna

Safumi Suzuki [*] and Satoshi Shibuya

Tokyo Institute of Technology, Graduate School of Science and Engineering, 2-12-1-S9-3 O-okayama, Meguro-ku, Tokyo 152-8552, Japan

[*] Email: suzuki.s.av@m.titech.ac.jp

Abstract: An increase in current responsivity of a terahertz (THz) detector using a broadband bow-tie antenna and an InAlAs/InGaAs high-electron-mobility transistor (HEMT) measurements was developed. We fabricated a HEMT THz detector with a reduced series resistance via etching control of the recess width. A high current responsivity of ≈13 *A/W* was obtained using an HEMT detector with a 45-*nm*-long gate. The transconductance was 2.35 *S/mm*, and the subthreshold slope was 89 *mV/dec*. The noise characteristics of the HEMT detector was also investigated. We measured the frequency dependence of the noise voltage, and a noise voltage of 5 *nV/Hz*$^{1/2}$ was obtained above a $1/f$ corner frequency of ≈500 *Hz*, which well agreed with the theoretical thermal noise of 4.5 *nV/Hz*$^{1/2}$ generated by drain conductance. We also measured the dependence of the noise voltage on the irradiated power of THz signal, and the noise equivalent power of 0.5 *pW/Hz*$^{1/2}$ was estimated from these measurements.

1. Introduction

Compact, high-responsivity, and low-noise detectors are key components for various applications of the THz waves [1-3]. Conventional Schottky barrier diode (SBD) detectors have been used in various THz applications. However, current responsivity R_i decreases in high-frequency operation because the area of the Schottky junction is small, which is a requirement for increasing the cutoff frequency. Recently, detectors that use field-effect transistors (FETs) have been intensively studied [4-7]. In contrast to the SBD detector, the cutoff frequency of a high-electron-mobility-transistor (HEMT) detector can be increased by reducing the gate length without reducing R_i. We proposed and fabricated a THz detector using an InGaAs composite-channel HEMT with a maximum transconductance, $g_{m.max}$, of 1.2 *S/mm* and achieved high R_i (5 *A/W*) [8]. Because R_i is proportional to $g_{m.max}$, increasing $g_{m.max}$ by decreasing the series resistance is effective to achieve high responsivity.

In the present study, we employed a high-indium-content and thick contact layer and controlled the side-recess spacing to reduce the series resistance. We measured the source–drain current during the wet-etching process to form the side recess and controlled the side-recess

spacing. A short side-recess spacing of 150 *nm* was achieved. We obtained a high $g_{m.max}$ value of 2.35 *S/mm* with a 45-*nm* gate length because of the reduced source resistance and high current responsivity of 13 *A/W*. We measured the frequency dependence of the noise voltage, and a noise voltage of 5 $nV/Hz^{1/2}$ was obtained over the $1/f$ corner frequency of ~500 *Hz*. We also measured the dependence of the noise voltage on the irradiated power of the THz signal, and a noise equivalent power (NEP) of 0.5 $pW/Hz^{1/2}$ was estimated from these measurements.

2. Device structure and detection mechanism

The schematic of the device structure of our HEMT THz detector is shown in Fig. 1(a). An InP-based InAlAs/InGaAs composite-channel HEMT with two-finger T-shaped gates was integrated at the center of a bow-tie antenna. The fabricated device was mounted on a silicon collimation lens and connected to each electrode by wire bonding. A metal–insulator–metal (MIM) capacitor with capacitance C_{MIM} was connected between the gate and the drain. It was shortened in the THz frequency and open for a direct current to provide a bias voltage.

Because the FET has diode-like characteristics in the I_d–V_{gs} characteristics, as shown in Fig. 1(b), irradiated THz waves can be detected by rectification. Although the detection mechanism is basically the same as that used for nonresonant plasmonic detection [4, 5], a high current responsivity is expected owing to the ballistic transport in a short-gate HEMT [8]. By irradiating a THz wave, an induced voltage is generated in the antenna. The induced voltage is applied between the source and gate, and the rectified THz current flows to the drain. This current is smoothed by the bonding-wire inductance that subsequently becomes the detection current. Using maximum transconductance $g_{m.max}$ and subthreshold slope *S.S.*, current responsivity R_i is roughly expressed as $R_i \approx g_{m.max}WR_a/S.S.$, where R_a is the antenna impedance and W is the gate width [8]. A high $g_{m.max}$ value with small subthreshold characteristics is required for high responsivity. Voltage responsivity R_v is obtained from R_i/g_d, where g_d is the drain conductance.
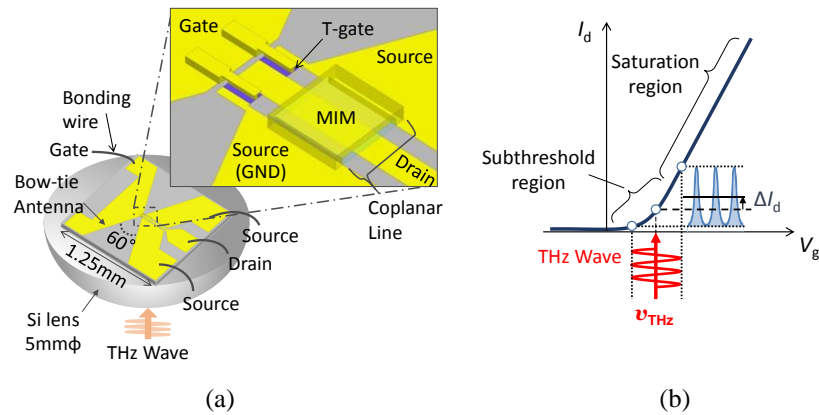

(a)   (b)

Fig. 1 (a) Schematic of the HEMT THz detector structure integrated with bow-tie antenna. The irradiated THz signal is received by the bow-tie antenna, and the received THz signal is input to the gate. (b) By using the nonlinearity in the I_d–V_{gs} characteristics, rectification of the THz signal is obtained.

3. Device fabrication and current-responsivity measurements

An epitaxial layer structure was grown using molecular beam epitaxy on semi-insulating (100) InP substrates. From the bottom to the top, the layers comprised a 200-*nm* InAlAs buffer, a 10-*nm* InGaAs composite channel, a 3-*nm* InAlAs spacer, a Si δ-doping of 5×10^{12} *cm*$^{-2}$, a 2-*nm* InAlAs barrier, a 3-*nm* InP etching stopper, a 10-*nm* layer of n$^+$-InAlAs (3×10^{19} *cm*$^{-3}$), a 40-*nm* layer of n$^+$-InGaAs (5×10^{19} *cm*$^{-3}$), and a 9-*nm* In-rich n$^+$-InGaAs (5×10^{19} *cm*$^{-3}$) contact layer. The two-dimensional electron gas mobility and density were 11670 *cm/V s* and 3.25×10^{12} *cm*$^{-2}$, respectively, obtained from the Hall measurements at room temperature. A thick (40 *nm*) n$^+$-InGaAs layer was employed to reduce the contact resistance by increasing the transfer length (effective contact length).

A tri-layer resist was used to form the T-shaped gate, and a Pt-buried-gate process was used to reduce the short-channel effect. The fabrication process is briefly described as follows. First, the device was isolated by wet chemical etching (H$_2$SO$_4$/H$_2$O$_2$/H$_2$O) using a ma-N resist (Micro Resist Technology) mask. The source, drain, and antenna electrodes (Ti/Pd/Au) were formed by a standard lift-off process using polymethyl methacrylate resist. The bow-tie angle was 60 °. The HEMT surface was covered with a SiO$_2$ film as an etching mask to form the gate-recess structure. A tri-layer resist (ZEP/PMGI/ZEP) was coated onto the SiO$_2$ film. The top and bottom ZEP layers were separately exposed using 50-*keV* electron beam irradiation. The gate pattern was replicated on the SiO$_2$ film using CF$_4$ inductively coupled plasma reactive-ion etching, and the gate-recess structure was formed by wet chemical etching. To reduce the source resistance, wet-etching control for short side-recess spacing was required. The details of the gate-recess formation are described in the next paragraph. Finally, a T-shaped gate electrode (Pt/Ti/Pt/Au) was deposited. The gate length was 45 *nm*.
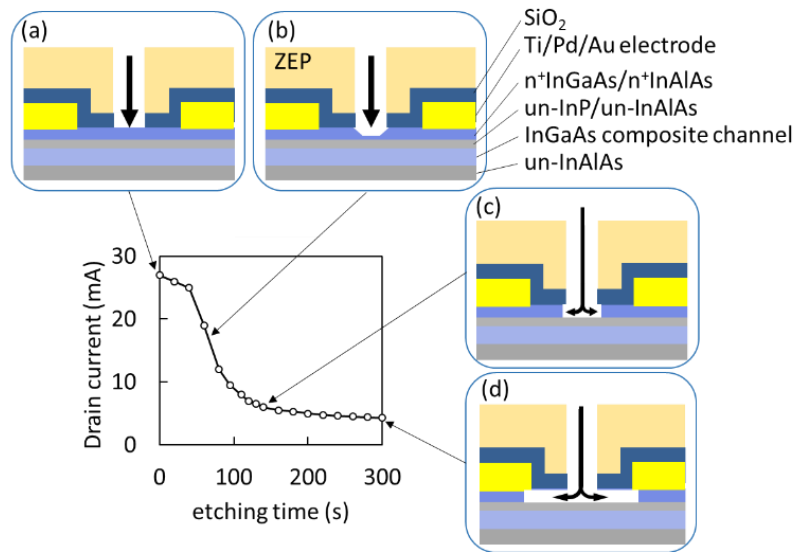

Fig. 2 Measured drain current as a function of the etching time. The corresponding cross-sectional views for various etching times are also shown.

In the gate-recess formation, the drain current was measured during the wet-etching process. The measured drain current as a function of the etching time is shown in Fig. 2. The source voltage was fixed at 1 *V*. First, the n$^+$InGaAs/n$^+$InAlAs contact layer, which has high conductivity, was etched using citric acid, due to which the current rapidly decreased. The corresponding cross-sectional view is shown in Figs. 2(a) and (b). Upon continued etching, the rate of current decrease became slow because the contact layer was completely separated, and current then flowed in the channel region, which has lower conductivity than the contact layer [Figs. 2(c) and (d)]. The etching stopped at (c) for the short side-recess spacing and reduction in the source resistance. A short side-recess spacing of 150 *nm* at one side was obtained in the (c) case. The gate width was 10 *μm*. The cross section of the T-gate and recess structure is shown in Fig. 3(a). The measured I_d–V_{gs} and transconductace characteristics are shown in Fig. 3(b). We obtained high $g_{m.max}$ (2.35 *S/mm*) by reducing the series resistance. The measured *S.S.* value was 89 *mV/dec*. We also fabricated a device with side-recess spacing of 550 *nm* at one side and obtained a $g_{m.max}$ value of 1.6 *S/mm*. Higher $g_{m.max}$ was obtained with the reduction in the series resistance because of the short side-recess spacing.
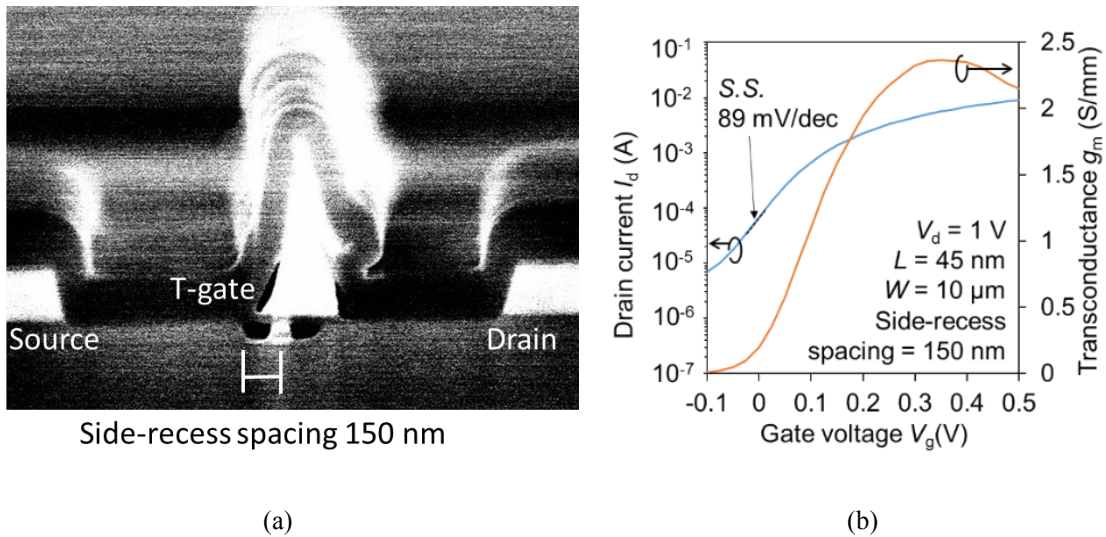

| (a) | (b) |

Fig. 3 (a) Cross section of the T-gate and recess structure. (b) I_d–V_{gs} and transconductance characteristics. High g_m and low *S.S.* were obtained with the reduction in the series resistance because of the control of the side-recess spacing and Pt-buried gate, respectively.

The experimental setup for measuring the detection current is shown in Fig. 4(a). A 280-*GHz* signal was generated by the frequency multiplier and focused on the HEMT detector using a Tsurupica^{TM} lens (the lens diameter was 10 *cm*, and the focal point was 10 *cm*). The HEMT detector was mounted at the center of a Si hemispherical lens (diameter: 5 *mm*) on a flat plane. A THz signal was irradiated from the substrate side through the lens. The output power from the frequency multiplier ranged from 6 *μW* to 19 *mW*. The 280-*GHz* signal was radiated from a horn antenna. The transmission losses due to air and lenses were negligible. Detection current flowed through a 1-Ω resistor. The voltage across the resistor was measured using a lock-in amplifier to reduce the surrounding noise. Drain bias V_d was 0.5 *V*. A subthreshold voltage of 50 *mV* was

applied to the gate. A maximum R_i value of 13 *A/W* was obtained in the low-received-power region. R_i decreased with the received power because of the degradation in the nonlinearity in the case of a large signal. The responsivity, estimated from the I_d–V_{gs} characteristics of the device, is shown in Fig. 4(b). The theoretical curve agreed well with the experimental data. As mentioned in Section 2, R_i and the cutoff frequency can be increased using a HEMT with a short gate and high $g_{m.max}$. Detectors with responsivity of ≈10 *A/W* and a cutoff frequency of 1 *THz* can be realized using a state-of-the-art HEMT, which has a gate length of 25 *nm* and g_{mmax} of 3.1 *S/mm* [9].
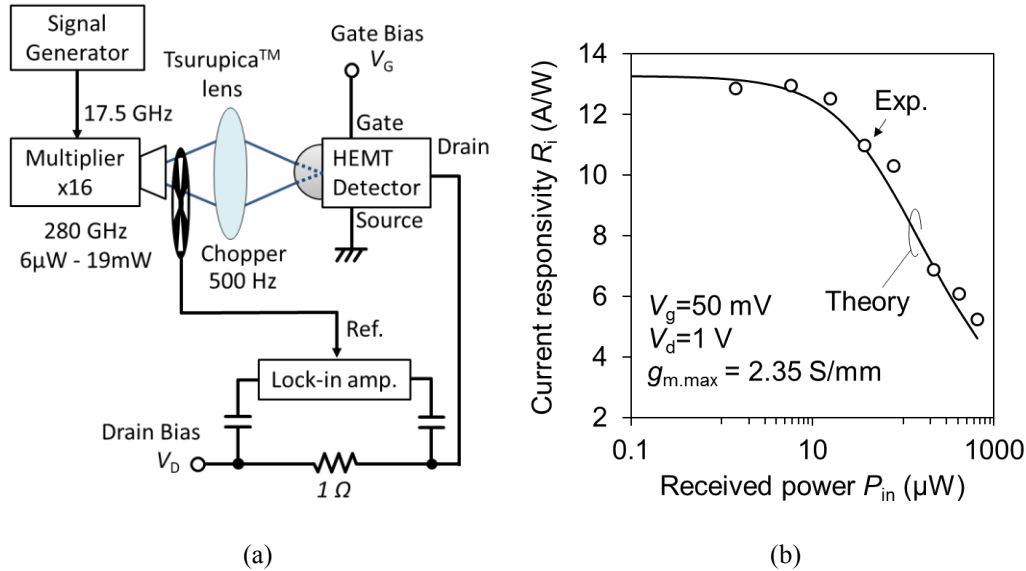

Fig. 4 (a) Measurement setup of a HEMT THz detector. A 280-*GHz* signal is generated by the multiplier. We measured the rectified current from the voltage drop at the 1-Ω resistor and used the lock-in amplifier for noise reduction. (b) Dependence of current responsivity R_i on received power P_{in}.

4. Noise Measurement

We also measured the noise characteristics of the HEMT detector. We used a HEMT detector with R_i = 8.3 *A/W* and drain conductance g_d of 0.83 *mS* in this measurement. The measurement setup is shown in Fig. 5. At first, the frequency characteristics of noise voltage V_n without THz-signal irradiation were measured by changing reference frequency f_{ref} of the lock-in amplifier. The measured result is shown in Fig. 6(a). In the low-frequency region, V_n is large due to the 1/*f* noise. The 1/*f* noise decreased with the frequency, and V_n became flat above the 1/*f* corner frequency of ≈500 *Hz*. V_n of 5 *nV/Hz*$^{1/2}$ was obtained above ≈500 *Hz*, which well agreed with the theoretical thermal noise of 4.5 *nV/Hz*$^{1/2}$ generated by a 0.83-*mS* drain conductance. Because the HEMT detector operated in the subthreshold region, the channel thermal noise was small, and the thermal noise due to the drain resistance was dominant.

Because of the THz-signal irradiation, a shot noise was generated by the detected current. We observed the dependence of the noise voltage on the irradiated power [Fig. 6(b)]. The measurement was performed with an f_{ref} of 10 kHz to neglect the $1/f$ noise. The shot noise decreased with decreasing irradiated power, and it crossed with a thermal noise of ≈ 5 $nV/Hz^{1/2}$, as mentioned earlier, at irradiated power of ≈ 0.3 μW. Therefore, the thermal noise was dominant in small-signal cases, and the NEP can be calculated using the simple equation NEP $= V_n/R_v$. R_v can be calculated by the following relationship, i.e., R_i/g_d. Using $R_v = 10$ kV/W and V_n of ≈ 5 $nV/Hz^{1/2}$, the NEP was obtained as ~ 0.5 $pW/Hz^{1/2}$. We achieved a very low NEP value with the HEMT THz detector, and a lower NEP of ≈ 0.3 $pW/Hz^{1/2}$ could be expected from a device with high R_i of 13 A/W, as discussed in Section 2.
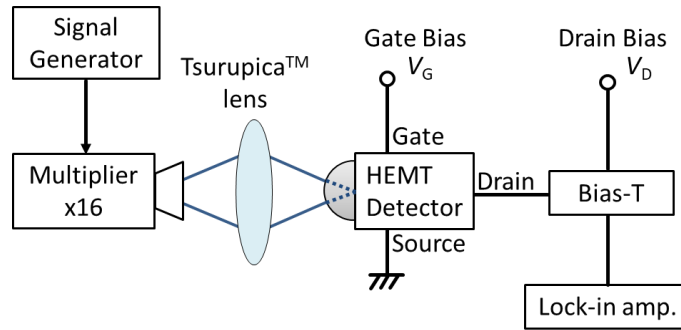

Fig. 5 Measurement setup for the noise characteristics of the HEMT detector. V_N is measured by the lock-in amplifier. An RF signal of over ≈ 100 Hz is input to the lock-in amplifier by the bias-T with a large inductance. The measurements are performed with and without the THz-signal source for frequency and received-power dependence characteristics, respectively. The frequency dependence is measured by changing the reference frequency of the lock-in amplifier.
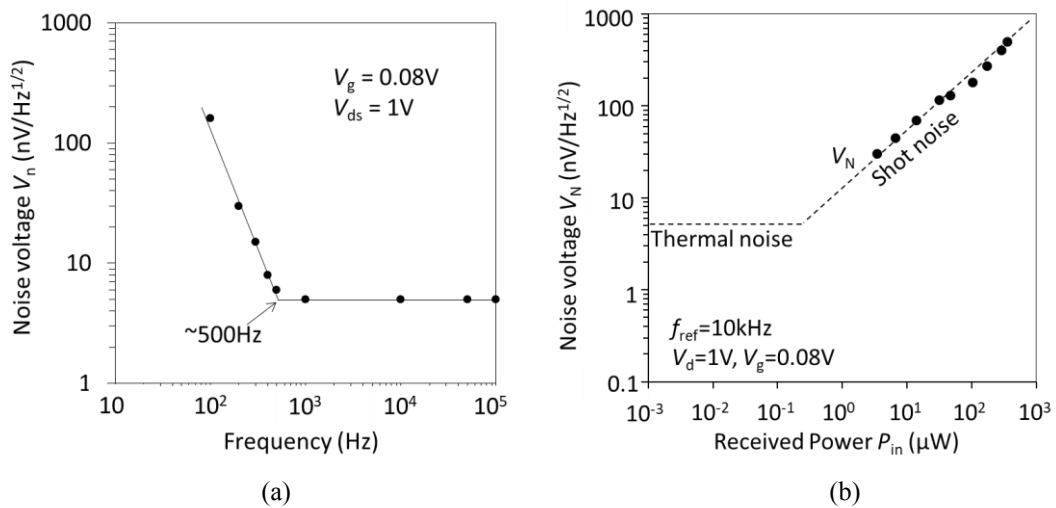

Fig. 6 (a) Frequency dependence of noise voltage V_N. (b) Dependence of noise voltage V_N on received power P_{in}.

5. Conclusions

The increase in current responsivity and noise-characteristic measurements were investigated by a THz detector using a broadband bow-tie antenna and an InAlAs/InGaAs HEMT. We fabricated a HEMT THz detector with reduced series resistance by etching control of the recess width. A high current responsivity of $\approx$13 *A/W* was obtained with the HEMT detector with a 45-*nm*-long gate. g_{mmax} was 2.35 *S/mm*, and *S.S.* was 89 *mV/dec*. We measured the frequency dependence of the noise voltage, and V_{N} of 5 *nV/Hz$^{1/2}$* was obtained above the 1/*f* corner frequency of $\approx$500 *Hz*, which well agreed with the theoretical thermal noise of 4.5 *nV/Hz$^{1/2}$* generated by the drain conductance. We also measured the dependence of the noise voltage on irradiated power of THz signal, and an NEP of 0.5 *pW/Hz$^{1/2}$* was estimated from these measurements.

Acknowledgements

References

[1]　M. Tonouchi. "Cutting-edge terahertz technology". *Nat. Photonics*, 1, 97–105 (2007).

[2]　T. Nagatsuma. "Terahertz Technologies: present and future". *IEICE Electron. Express*, 8, 1127–1142 (2011).

[3]　M. Hangyo. "Development and future prospects of terahertz technology". *Jpn. J. Appl. Phys.*, 54, 120101 (2015).

[4]　T. Watanabe, S. B. Tombet, Y. Tanimoto, et al. "Ultrahigh sensitive plasmonic terahertz detector based on an asymmetric dual-grating gate HEMT structure," *Solid-State Electron*. 78, 109–114 (2012).

[5]　W. Knap, V. Kachorovskii, Y. Deng, et al. "Nonresonant detection of terahertz radiation in field effect transistors". *J. Appl. Phys.*, 91, 9346–9353 (2002).

[6]　E. Ojefors, A. Lisauskas, D. Glaab, et al. "Terahertz imaging detectors in CMOS technology". *J. Infrared Milli. Terahertz Waves*, 30, 1269–1280 (2009).

[7]　M. Sakhno, F. Sizov, and A. Golenkov. "Uncooled THz/sub-THz Rectifying Detectors: FET vs. SBD". *J. Infrared Milli. Terahertz Waves*, 34, 798–814 (2013).

[8]   S. Suzuki, T. Nukariya, Y. Ueda, et al. "High Current Responsivity and Wide Modulation Bandwidth Terahertz Detector Using High-Electron-Mobility Transistor for Wireless Communication". *J. Infrared Milli. Terahertz Waves*, 37, 658–667 (2016).

[9]   X. Mei, W. Yoshida, M. Lange, et al. "First Demonstration of Amplification at 1 THz Using 25-nm InP High Electron Mobility Transistor Process". *IEEE Electron. Device Lett*., 36, 327–329 (2015).